Lee Young-gun (Orcid ID: 0000-0003-0460-455X)
Baik Kyoungwon (Orcid ID: 0000-0001-7215-375X)
Lee Phil Hyu (Orcid ID: 0000-0001-9931-8462)
Ye Byoung Seok (Orcid ID: 0000-0003-0187-8440)

Effects of Alzheimer's and Lewy Body Disease Pathologies on Brain Metabolism

Young-gun Lee, MD, PhD[1,†], Seun Jeon, PhD[1,2,†], Mincheol Park, MD[1], Sung Woo Kang, MD[1], So Hoon Yoon, MD[1], Kyoungwon Baik, MD[1], Phil Hyu Lee, MD, PhD[1,3], Young Ho Sohn, MD, PhD[1], Byoung Seok Ye, MD, PhD[1], and the Alzheimer's Disease Neuroimaging Initiative*

[†]These authors contributed equally to this work.

Author affiliations:

[1]Department of Neurology, Yonsei University College of Medicine, Seoul, South Korea

[2]Brain Research Institute, Yonsei University College of Medicine, Seoul, South Korea

[3]Severance Biomedical Science Institute, Yonsei University College of Medicine, Seoul, South Korea

* Data used in the preparation of this article were obtained from the Alzheimer's Disease Neuroimaging Initiative (ADNI) database (adni.loni.usc.edu). The investigators of the ADNI contributed to the design and implementation of the ADNI and/or provided data, but they did not participate in the analysis or writing of this report. A complete list of the ADNI investigators can be found at http://adni.loni.usc.edu/wpcontent/uploads/how_to_apply/ADNI_Acknowledgement_List.pdf

Correspondence to: Byoung Seok Ye

Department of Neurology, Yonsei University College of Medicine, 50 Yonseiro, Seodaemun-gu, Seoul, 03722, South Korea

This article has been accepted for publication and undergone full peer review but has not been through the copyediting, typesetting, pagination and proofreading process which may lead to differences between this version and the Version of Record. Please cite this article as doi: 10.1002/ana.26355

E-mail: romel79@gmail.com

Running title: Autopsy-validation study of an ADNI cohort

Word count: 3,465

Abstract

Objective: This study aimed to determine the pattern of ^{18}F-fluorodeoxyglucose positron emission tomography (FDG-PET) related to postmortem Lewy body disease (LBD) pathology in clinical Alzheimer's disease (AD).

Methods: FDG-PET scans were analyzed in 62 autopsy-confirmed patients and 110 controls in the Alzheimer's Disease Neuroimaging Initiative. Based on neuropathologic evaluations on Braak's stage for neurofibrillary tangle, Consortium to Establish a Registry for AD score for neuritic plaque, and Lewy-related pathology, subjects were classified into AD(-)/LBD(-), AD(-)/LBD(+), AD(+)/LBD(-), and AD(+)/LBD(+) groups. The association between postmortem LBD and AD pathologies and antemortem brain metabolism was evaluated.

Results: AD and LBD pathologies had significant interaction effects to decrease metabolism in the cerebellar vermis, bilateral caudate, putamen, basal frontal cortex, and anterior cingulate cortex in addition to the left side of entorhinal cortex and amygdala; and those to increase metabolism in the bilateral parietal and occipital cortices. LBD pathology was associated with hypermetabolism in the cerebellar vermis, bilateral putamen, anterior cingulate cortex, and basal frontal cortex, corresponding to the LB-related hypermetabolic patterns. AD pathology was associated with hypometabolism in the bilateral hippocampus, entorhinal cortex, and posterior cingulate cortex regardless of LBD pathology, while LBD pathology was associated with hypermetabolism in the bilateral putamen and anterior cingulate cortex regardless of AD pathology.

Interpretation: Postmortem LBD and AD pathologies had significant interaction effects on the antemortem brain metabolism in clinical AD patients. Specific metabolic patterns related to AD and LBD pathologies could be elucidated when simultaneously considering the two pathologies.

Keywords: Lewy body disease; Alzheimer's disease; Metabolic pattern;

^{18}F□fluorodeoxyglucose PET.

Introduction

In the two most common forms of neurodegenerative dementia, Alzheimer's disease (AD) and Lewy body disease (LBD), mixed pathology is found in more than 50% of the patients.[1-3] In AD, the presence of LBD pathology is associated with younger symptom onset,[4] parkinsonism,[5] worse cognition,[6] and faster progression.[7] However, even with the evidence of mixed pathologies in cognitively impaired patients, the lack of sensitive *in vivo* biomarkers for LBD pathology prevents precise diagnoses in clinical settings. Therefore, it is not uncommon for patients who were clinically diagnosed with AD to show mixed pathologies of LBD during autopsy.[8] Failure to evenly distribute patients with mixed LBD may lead to inaccurate evaluation of new therapeutic agents in clinical trials for AD.

Metabolic changes on ^{18}F-fluorodeoxyglucose (FDG)-positron emission tomography (PET) have clinical implications for the differential diagnosis of neurodegenerative dementia.[9] Hypometabolism in the temporal, parietal, and medial temporal cortex is the typical metabolic pattern of clinically diagnosed AD patients,[10,11] and occipital hypometabolism[12] and posterior cingulate island signs[13] are observed in clinically diagnosed patients with dementia with Lewy bodies (DLB) (Supplementary Figure 1). Hypermetabolism in the basal ganglia, motor cortex, and cerebellum has been reported in LBD, including idiopathic RBD,[14] Parkinson's disease (PD),[15,16] and DLB,[17,18] and these LB-related metabolic patterns (LBRPs) may enhance the diagnostic accuracy of LBD.[19] However, to the best of our knowledge, metabolic changes related to AD and LBD have not been elucidated in autopsy-confirmed patients.

In-vivo detection of mixed pathologies in patients with neurodegenerative dementia would have clinical importance for treatment and predicting prognosis. In this study, we evaluated the metabolic changes of antemortem FDG-PET related to AD and LBD pathologies on postmortem autopsies from the Alzheimer's Disease Neuroimaging Initiative

(ADNI) cohort, which were aimed to include dementia or mild cognitive impairment (MCI) due to AD.[20] We hypothesized that AD and LBD pathologies could have significant interaction effects on brain metabolism,[21-25] and pathology-specific metabolic patterns could be identified after considering these interaction effects.

Methods

Study subjects

Our data were obtained from the ADNI database (http://adni.loni.usc.edu/). The ADNI is a longitudinal study launched in 2003 as a public-private partnership, to assess biomarkers for the progression of MCI and early AD. The inclusion and exclusion criteria are available at the ADNI protocol (http://adni.loni.usc.edu/methods/documents/). Briefly, diagnosis of dementia was based on the National Institute of Neurological and Communicative Disorders and Stroke and the Alzheimer's Disease and Related Disorders Association criteria for probable AD. Individuals with MCI had preserved general cognition and functional performance and were required to have an abnormal memory function, Mini-Mental State Examination (MMSE) between 24 and 30, and a clinical dementia rating (CDR®) score of 0.5. General cognitive status was measured using the MMSE and CDR-sum of boxes (CDR-SOB).

Autopsy consent and neuropathologic evaluation were established by a Neuropathology Core (NPC) of the ADNI database. As of July 2021, autopsy results from 81 subjects were available in the ADNI database. After excluding the subjects who had not received FDG-PET (n=17) and those who maintained normal cognition until autopsy (n=2), a total of 62 subjects were included in the analysis. Among cognitively normal participants, 352 received FDG-PET. We included subjects who were followed up for >2 years, had maintained normal cognition, and had normal CSF p-tau/Aβ ratios (<0.028).[26] After excluding low-quality MRI and PET images (n=4), 110 control subjects were included.

Neuropathologic assessment

Neuropathologic evaluation of the ADNI database[27] follows the National Institute on Aging and Alzheimer's Association (NIA-AA) guidelines[28] and DLB Consortium classification.[29] Details of the neuropathologic protocol of the ADNI-NPC can be found in the ADNI database (http://adni.loni.usc.edu/). AD neuropathology was evaluated using the Thal phase for Aβ plaques, the Braak and Braak stage for neurofibrillary tangles (NFTs) or tau burden, and the Consortium to Establish a Registry for AD (CERAD) score for neuritic plaques.[27] Aβ plaques have little effects on the clinical features in LBD as well as AD,[22] and pathologic diagnosis of mixed AD with LBD could be overestimated by including LBD patients with high Aβ load but low burden of tau or neuritic plaques. Therefore, we defined the presence of AD pathology using the previously reported modified NIA-AA criteria based on NFT Braak stages and CERAD scores.[3,30] In specific, subjects were classified into: (i) no AD = NFT(0)/CERAD(0), NFT(I-II)/CERAD(0); (ii) low AD = NFT(I-II)/CERAD(1-3), NFT(III-IV)/CERAD(0-1); (iii) intermediate AD = NFT(III-IV)/CERAD(2-3), NFT(V-VI)/CERAD(1); and (iv) high AD = NFT(V-IV)/CERAD(2-3). Subjects with intermediate or high AD pathology were treated as having AD pathology.

LBD neuropathologic changes were evaluated based on the degree and distribution of Lewy-related pathology in six stages: none, brainstem-predominant, limbic (transitional), neocortical (diffuse), amygdala-predominant, or olfactory-only.[28,29,31] Dichotomization of LBD pathology was based on the presence of brainstem-predominant, limbic, and neocortical Lewy-related pathology, which are mostly related to the core clinical features of LBD.[23,32] According to dichotomized AD and LBD pathologies, autopsy-confirmed subjects were grouped into four groups: AD(-)/LBD(-), AD(-)/LBD(+), AD(+)/LBD(-), and AD(+)/LBD(+). The control subjects were considered to have AD(-) and LBD(-).

MRI image processing

We used the FMRIB Software Library (FSL, http://www.fmrib.ox.ac.uk/fsl) for image processing. Each subject's T1-weighted images were corrected for intensity inhomogeneity, skull-stripped, and registered to the ADNI-Montreal Neurological Institute (MNI) atlas, which is a T1-weighted template for older adults.[33,34] The brain tissues were classified into white matter, gray matter (GM), or CSF based on the hidden-Markov random field model and the associated expectation-maximization algorithm.[35] The GM probability map obtained from this algorithm was non-linearly transformed into the ADNI-MNI template. The striatal regions were segmented using the FMRIB integrated registration and segmentation tool (FIRST) algorithm.[36] We included the striatal regions of interest in the GM class. Then, we averaged all of the individual GM probability maps and assigned each voxel into either the foreground or background by binarizing above 30% of the map to generate a study-specific GM mask. For voxel-based MRI statistical analyses, an additional modulation step for the GM probability map was included to keep the total GM amount constant, regardless of local expansion or contraction due to image normalization.

FDG-PET image processing

We linearly registered each subject's FDG-PET image to individual T1-weighted MRI using a rigid body transformation. To generate standardized uptake value ratio (SUVR) maps, we used the cerebellar cortex as a reference region. Then, we spatially normalized the SUVR maps to the ADNI-MNI template using non-linear warping fields acquired in the T1-weighted image processing stage, and then smoothed them using 6-mm full width at a half-maximum Gaussian kernel. To calculate the FDG subject residual profile (FDG-SRP), each data was transformed into logarithmic form, and the data matrix was centered by subtracting each subject mean and the group mean voxel profile from the data.[37] To extract individual LBRP scores, we adopted LBRPs from the Severance Hospital dataset, as described in the previous study.[19] Briefly, to capture the regional covariance patterns associated with disease progression and severity in the LBD spectrum, we computed the principal component coefficients using reduced singular value decomposition from spatially normalized FDG-SRP images of the Severance Hospital dataset (55 DLB patients and 49 healthy controls). The LBRP scores were then computed by applying the first principal component coefficient map that is associated with the LBRPs to individual FDG-SRP images of the ADNI dataset within the GM mask.

Quality assurance

For quality assurance, results from the image processing stages were visually inspected by three researchers (Y. Lee, S. Jeon, and B.S. Ye) who were blinded to the subject information. We excluded seven subjects from the original dataset due to image processing errors in brain masking, tissue classification, and volume registration. Finally, a total of 172 subjects were included in the statistical analysis.

Statistical analysis

Statistical analyses of the demographic and clinical data were performed using IBM SPSS version 26.0 (SPSS Inc., Chicago, IL, USA), and those for voxel-based statistics were performed using the SurfStat toolbox (http://www.math.mcgill.ca/keith/surfstat). An analysis of variance, Kruskal-Wallis, and chi-square tests were used to compare the demographic variables between the control group and the four autopsy-confirmed groups. General linear models for LBRP and FDG-SRP were performed using AD and LBD pathologies and their interaction as predictors to evaluate the effect of each pathology on brain metabolism.

Covariates included the age at FDG scan, sex, and education. We also compared the LBRP and FDG-SRPs between the control group and the four disease groups using general linear models after controlling for age, sex, and education. In the voxel-based analyses, false discovery rate (FDR) methods were used to correct for multiple comparisons across the voxels. We displayed voxel-wise statistical outcomes, including effect sizes (r, d), within statistically significant areas (corrected $p < 0.05$, FDR) on the ADNI-MNI stereotaxic space in neurological convention. To interpret the patterns of independent and interaction effects from AD and LBD pathologies, we selected 15 regions of interest (ROIs) where there were significant pathology-related effects or group differences. For the ROI-based analyses, we used the median value of the selected ROIs based on the automated anatomical labeling atlas 3.[38]

Data availability

All data used in this study can be obtained from the ADNI website (http://adni.loni.usc.edu/).

Results

Demographic and clinical characteristics

The demographic and clinical characteristics are shown in Table 1. The control subjects did not differ in age at the time of FDG-PET, sex, and education compared to the four neuropathologic groups. On average, the autopsy was conducted at the age of 84.1 years and 4.9 years after the FDG-PET acquisition. Age at autopsy and interval from FDG-PET to autopsy were comparable between the four neuropathologic groups. Neuropathologic groups had lower MMSE scores and higher CDR-SOB compared to the control group. Among neuropathologic groups, the MMSE score was the lowest in AD(+)/LBD(+) group and the highest in AD(-)/LBD(-) group. Detailed neuropathologic findings of the neuropathologic groups are described in Supplementary Table 1. Seven of 10 subjects in the AD(-)/LBD(-) group had neuropathologic diagnoses, including frontotemporal lobar degeneration (FTLD), argyrophilic grain disease (AGD), primary age-related tauopathy (PART), and aging-related tau astrogliopathy (ARTAG), while three did not have a specific diagnosis (Supplementary Table 2).

Effects of AD and LBD pathologies on brain metabolism

Significant interaction effects of AD and LBD pathologies were observed in the cerebellar vermis, bilateral caudate, putamen, basal frontal cortex, anterior cingulate cortex, parietal cortex, and occipital cortex in addition to the left entorhinal cortex and amygdala (Figure 1). After considering the interaction effects, AD pathology was associated with hypometabolism in the bilateral hippocampus, caudate, entorhinal cortex, posterior cingulate cortex, basal frontal cortex, and parietal cortex, in addition to the left amygdala, while it was associated with hypermetabolism in the cerebellar vermis, bilateral motor cortex, and medial occipital cortex. LBD pathology was associated with hypermetabolism in the cerebellar vermis, bilateral putamen, anterior cingulate cortex, and basal frontal cortex, while it was associated with hypometabolism in the bilateral parietal cortex and posterior cingulate cortex.

Comparison of brain metabolism with the control group

When the brain metabolism of each neuropathologic group was compared to the control group, AD(-)/LBD(+), AD(+)/LBD(-), and AD(+)/LBD(+) groups commonly had hypermetabolism in the cerebellum, pallidum, and motor cortex, while they had hypometabolism in the inferior/lateral temporal and parietal cortices (Figure 2). The AD(+)/LBD(-) and AD(+)/LBD(+) groups had hypometabolism in the hippocampus/entorhinal cortex and hypermetabolism in the medial occipital cortex, while the

AD(-)/LBD(+) group did not. Meanwhile, the AD(-)/LBD(+) and AD(+)/LBD(+) groups had hypermetabolism in the putamen, while the AD(+)/LBD(-) group did not. In the bilateral caudate and left amygdala, the AD(-)/LBD(+) group had hypermetabolism; the AD(+)/LBD(+) group had hypometabolism; and the AD(+)/LBD(-) group did not have significant metabolic changes. Compared to the control group, AD(-)/LBD(-) group had hypometabolism localized in the hippocampus/entorhinal cortex.

ROI-based comparison of brain metabolism

To capture the patterns of independent and interaction effects from AD and LBD, we presented the regional metabolism in the 15 ROIs (Table 2 and Figure 3). Compared to the sum of mean metabolism in the AD(+)/LBD(-) and AD(-)/LBD(+) groups, the AD(+)/LBD(+) group had more decreased metabolism in the bilateral caudate, and left side of amygdala and entorhinal cortex ROIs, but more increased metabolism in the bilateral occipital cortex and parietal cortex ROIs. Hypometabolism in the medial occipital cortex ROI and hypermetabolism in the bilateral basal frontal cortex, caudate, and hippocampus, and left side of amygdala and entorhinal cortex ROIs were observed only in the AD(-)/LBD(+) group, but not in the AD(+)/LBD(-) and AD(+)/LBD(+) groups. AD pathology was associated with hypometabolism in the bilateral hippocampus, posterior cingulate cortex, and left entorhinal cortex ROIs regardless of LBD pathology, while LBD pathology was associated with hypermetabolism in the bilateral putamen and anterior cingulate cortex ROIs regardless of AD pathology.

Lewy body-related metabolic patterns in neuropathologic groups and control group

When the effects of AD and LBD on LBRP were evaluated, both pathologies had significant independent and interaction effects on the LBRP (Table 3). The general linear model for

LBRP showed that the AD(-)/LBD(+), AD(+)/LBD(-), and AD(+)/LBD(+) groups had higher LBRP than did the control and AD(-)/LBD(-) groups (Supplementary Table 3). In the AD(+)/LBD(-) group, GM density in the right insula, bilateral posterior putamen, frontal, temporal, and occipital cortices showed a significant correlation with the LBRPs (Supplementary Figure 2). When the AD(+)/LBD(-) group was further divided into AD patients with amygdala-predominant or olfactory-only Lewy-related pathology (AD(+)/Lewy(+); n = 10) and those without (AD(+)/Lewy(-); n = 19), both groups exhibited increased metabolism in the cerebellum, pallidum, and motor cortex compared to the control group. Although the AD(+)/Lewy(+) group had relatively more hypermetabolism in the cerebellum, pallidum, and putamen and higher LBRPs compared to the AD(+)/Lewy(-) group, statistical significance was not reached (Supplementary Figure 3 and Supplementary Table 4).

Discussion

Herein, we evaluated the antemortem brain metabolic patterns related to the postmortem AD and LBD pathologies. The major findings of our study were as follows. First, AD and LBD pathologies had regionally distinct interaction effects on brain metabolism. Second, after considering the interaction effects, LBD pathology was associated with hypermetabolism in the cerebellar vermis, bilateral putamen, anterior cingulate cortex, and basal frontal cortex. Third, AD pathology was associated with hypometabolism in the bilateral hippocampus, entorhinal cortex, caudate, posterior cingulate cortex, basal frontal cortex, parietal cortex, and left amygdala. Taken together, our results suggest that AD and LBD pathologies are interactively associated with brain metabolic changes, and specific metabolic patterns related to AD and LBD could be elucidated when simultaneously considering the two pathologies.

Our first major finding was that AD and LBD pathologies had regionally distinct interaction effects on brain metabolism. First, decremental interacting effects on the cerebellar vermis, bilateral caudate, putamen, basal frontal cortex, anterior cingulate cortex, and left side of entorhinal cortex and amygdala metabolism suggest that two pathologies may aggravate synaptic dysfunction. Cross-fibrillation between tau and α-synuclein could be a possible candidate for these interaction effects to aggravate their spreading and neuronal degeneration.[39-41] On the other hand, incremental interacting effects were observed in the bilateral parietal and occipital metabolism. In specific, the metabolism of parietal and occipital cortices in AD(+)/LBD(+) group was greater than the sum of metabolism in AD(+)/LBD(-) and AD(-)/LBD(+) groups. Also, medial occipital hypometabolism was observed only in AD(-)/LBD(+) group, but not in AD(+)/LBD(+). This incremental interaction was interpreted as pathologic rather than compensatory and could be related to previously reported neuronal hyperexcitability in animal models of tau and α-synuclein co-pathologies.[42,43] Based on the regionally distinct interaction effects between AD and LBD pathologies, it is suggested that metabolic changes due to neurodegenerative diseases cannot be measured by unidirectional hypometabolism.

Our second major finding was that after considering the significant interaction effects of AD and LBD on brain metabolism, LBD pathology was associated with hypermetabolism in the cerebellar vermis, bilateral putamen, anterior cingulate cortex, and basal frontal cortex. This hypermetabolic pattern overlaps with the previously reported PD-[15,16] or DLB-related metabolic patterns.[17-19] However, to our knowledge, the present study is the first autopsy-based validation of the association between LBD pathology and LBRPs. Furthermore, hypermetabolism in the bilateral putamen and anterior cingulate cortex was evident in both AD(-)/LBD(+) and AD(+)/LBD(+) groups (Figure 3 and Table 2), suggesting that they could be useful biomarkers for the presence of LBD pathology regardless of AD pathology. In contrast, occipital hypometabolism and relative preservation of posterior cingulate cortex metabolism were evident only in AD(-)/LBD(+) group, but not in AD(+)/LBD(+) group (Figure 3). Furthermore, independent effect of LBD pathology on occipital metabolism was not significant, in contrast to the negative effect on posterior cingulate cortex (Table 2). This may explain the low diagnostic sensitivity of cingulate island sign and occipital hypometabolism in clinical settings,[12,13] especially in patients with concomitant AD pathology.

Our third major finding was that after considering the significant interaction effects of AD and LBD on brain metabolism, AD pathology was associated with hypometabolism in the bilateral caudate, hippocampus, entorhinal cortex, posterior cingulate cortex, basal frontal cortex, parietal cortex, and left amygdala. Among these brain regions, hypometabolism in the bilateral hippocampus, posterior cingulate cortex, and left entorhinal cortex was observed in the AD(+)/LBD(-) and AD(+)/LBD(+) groups, suggesting that they could be metabolic hallmarks of AD regardless of the presence of LBD pathology (Figure 3). Although the effect size of AD pathology on brain metabolism was the highest in both left entorhinal cortex and bilateral posterior cingulate cortex (Table 2), as the AD(-)/LBD(+) group also showed hypometabolism in the posterior cingulate cortex compared to the control group (Figure 2), hypometabolism on the left side of entorhinal cortex could be a better biomarker for AD.[17]

Notably, AD pathology was associated with hypermetabolism of the cerebellar vermis, bilateral motor cortex, medial occipital cortex, and pallidum (Figure 1). Furthermore, in addition to the AD(-)/LBD(+) and AD(+)/LBD(+) groups, the AD(+)/LBD(-) group also showed hypermetabolism in the cerebellar vermis, bilateral pallidum, and motor cortex (Figure 2). There could be several hypotheses to explain these results. First, the hypermetabolic changes in the AD(+)/LBD(-) group could be attributed to the limited Lewy-related pathology observed in 10 of 29 patients (34.5%) in the AD(+)/LBD(-) group (Supplementary Table 1). In the AD(+)/LBD(-) group, LBRPs were correlated with lower

GM density in the right insula, bilateral posterior putamen, frontal, temporal, and occipital cortices, where GM changes were observed in LBDs,[44-46] with relative sparing of the entorhinal cortex, vermis, and anterior cingulate cortex (Supplementary Figure 2). Second, hypermetabolic brain changes may not be specific to Lewy-related pathology but also be related to AD pathology. To test this hypothesis, we compared the metabolic changes between AD(+)/Lewy(-) and AD(+)/Lewy(+) within the AD(+)/LBD(-) group (n = 29). The AD(+)/Lewy(-) group exhibited increased metabolism in the cerebellum, pallidum, and motor cortex compared to the control group (Supplementary Figure 3) and had comparable LBRPs than AD(+)/Lewy(+) group (Supplementary Table 4). There could be several hypothetical mechanisms for the increased metabolism in these pure AD patients. First, tau-related disruption of inhibitory network could induce relative hypermetabolism.[47] Second, metabolism could be relatively preserved due to the lack of tau pathology in the cerebellum and motor cortex. Third, synergistic interaction between tau and limited Lewy-related pathology in brain regions where neuropathologic examinations are not routinely conducted could also be a possible candidate. However, since hypermetabolism involving the putamen was observed only in the AD(+)/Lewy(+) group but not in the AD(+)/Lewy(-) group, it could be a biomarker specific for Lewy-related pathology in AD patients. Future autopsy studies with sufficiently large sample sizes with post-mortem global screening of Lewy-related pathology are needed.

Although the underlying pathologies of AD(-)/LBD(-) were heterogeneous, most of the cases (70%) were diagnosed as having tauopathies, including ARTAG and primary tauopathy, such as FTLD, AGD, and PART (Supplementary Table 2). Clinical presentations of these tau-related pathologies are considered to be milder than AD, consistent with the limited hypometabolism of entorhinal cortex observed in the AD(-)/LBD(-)group compared to other neuropathology groups (Figure 2A).[48-50] Our results suggest that limited entorhinal/hippocampal hypometabolism could be an imaging feature of non-AD tauopathies mimicking clinical AD.

This study had several limitations. First, there were time intervals from FDG-PET scanning to autopsy. We considered that the pathologic burden at the time of FDG-PET scanning would be similar to that in the postmortem autopsy results. Second, due to the rarity of autopsy data, our results were based on small sample size. Also, since we combined the subjects without any Lewy-related pathology and those with limited Lewy-related pathology into a LBD(-) group, we could not analyze the effects of various Lewy-related pathology distributions on metabolic patterns. Future studies with a large sample size are warranted using different categorizations by the distribution of Lewy-related pathology to reveal the effects of LBD staging on metabolism. Despite these limitations, we found that mixed LBD pathologies are common and contribute to brain metabolic changes in clinical AD patients.

In conclusion, we found significant interaction effects of postmortem AD and LBD pathologies on antemortem brain metabolism and demonstrated AD- and LBD-related metabolic changes in patients with the clinical diagnosis of AD. Since our results were based on group-level findings, future studies with a large sample size are needed to investigate the diagnostic implication of AD- and LBD-related metabolic patterns on an individual level.

Acknowledgements: The authors are grateful to all of the participants in this study. Data collection and sharing for this project were funded by the ADNI (National Institutes of Health Grant U01 AG024904) and DOD ADNI (Department of Defense award number W81XWH-12-2-0012). ADNI is funded by the National Institute on Aging, the National Institute of Biomedical Imaging and Bioengineering, and through generous contributions from the following groups: AbbVie, Alzheimer's Association; Alzheimer's Drug Discovery Foundation; Araclon Biotech; BioClinica, Inc.; Biogen; Bristol-Myers Squibb Company; CereSpir, Inc.; Cogstate; Eisai Inc.; Elan Pharmaceuticals, Inc.; Eli Lilly and Company; EuroImmun; F. Hoffmann-La Roche Ltd and its affiliated company Genentech, Inc.; Fujirebio; GE Healthcare; IXICO Ltd.; Janssen Alzheimer Immunotherapy Research & Development, LLC.; Johnson & Johnson Pharmaceutical Research & Development LLC.; Lumosity; Lundbeck; Merck & Co., Inc.; Meso Scale Diagnostics, LLC.; NeuroRx Research; Neurotrack Technologies; Novartis Pharmaceuticals Corporation; Pfizer Inc.; Piramal Imaging; Servier; Takeda Pharmaceutical Company; and Transition Therapeutics. The Canadian Institutes of Health Research provided funding to support the ADNI clinical sites in Canada. Private sector contributions are facilitated by the Foundation for the National Institutes of Health (http://www.fnih.org/). The grantee organization is the Northern California Institute for Research and Education, and the study is coordinated by the Alzheimer's Therapeutic Research Institute at the University of Southern California. ADNI data are disseminated by the Laboratory for Neuro Imaging at the University of Southern California. This research was supported by a grant of the Korea Health Technology R&D Project through the Korea Health Industry Development Institute (KHIDI), funded by the Ministry of Health & Welfare and Ministry of Science and ICT, Republic of Korea (grant number: HU20C0511020021) and by the National Research Foundation of Korea (NRF) grant funded by the Korea government (MSIT) (No. 2022R1C1C2011227).

Author contributions: YL, SJ, and BSY contributed to conception and design of the study; YL, SJ, and BSY contributed to the acquisition and analysis of data; YL, SJ, MP, SWK, SHY, KB, PHL, YHS, and BSY contributed to drafting the text or preparing the figures.

Potential conflict of interest: The authors declare that they have no conflict of interest.

References

1. Lippa CF, Fujiwara H, Mann DM, et al. Lewy bodies contain altered alpha-synuclein in brains of many familial Alzheimer's disease patients with mutations in presenilin and amyloid precursor protein genes. Am J Pathol 1998;153(5):1365-1370.
2. Hamilton RL. Lewy bodies in Alzheimer's disease: a neuropathological review of 145 cases using alpha-synuclein immunohistochemistry. Brain Pathol 2000;10(3):378-384.
3. Irwin DJ, Grossman M, Weintraub D, et al. Neuropathological and genetic correlates of survival and dementia onset in synucleinopathies: a retrospective analysis. Lancet Neurol 2017;16(1):55-65.
4. Chung EJ, Babulal GM, Monsell SE, Cairns NJ, Roe CM, Morris JC. Clinical Features of Alzheimer Disease With and Without Lewy Bodies. JAMA Neurol 2015;72(7):789-796.
5. Forstl H, Burns A, Luthert P, Cairns N, Levy R. The Lewy-body variant of Alzheimer's disease. Clinical and pathological findings. Br J Psychiatry 1993;162:385-392.
6. Azar M, Chapman S, Gu Y, Leverenz JB, Stern Y, Cosentino S. Cognitive tests aid in clinical differentiation of Alzheimer's disease versus Alzheimer's disease with Lewy body disease: Evidence from a pathological study. Alzheimers Dement 2020;16(8):1173-1181.
7. Kraybill ML, Larson EB, Tsuang DW, et al. Cognitive differences in dementia patients with autopsy-verified AD, Lewy body pathology, or both. Neurology 2005;64(12):2069-2073.
8. Walker L, McAleese KE, Thomas AJ, et al. Neuropathologically mixed Alzheimer's and Lewy body disease: burden of pathological protein aggregates differs between

clinical phenotypes. Acta Neuropathol 2015;129(5):729-748.

9. Mosconi L, Tsui WH, Herholz K, et al. Multicenter standardized 18F-FDG PET diagnosis of mild cognitive impairment, Alzheimer's disease, and other dementias. J Nucl Med 2008;49(3):390-398.

10. Mattis PJ, Niethammer M, Sako W, et al. Distinct brain networks underlie cognitive dysfunction in Parkinson and Alzheimer diseases. Neurology 2016;87(18):1925-1933.

11. Anchisi D, Borroni B, Franceschi M, et al. Heterogeneity of brain glucose metabolism in mild cognitive impairment and clinical progression to Alzheimer disease. Arch Neurol 2005;62(11):1728-1733.

12. Minoshima S, Foster NL, Sima AA, Frey KA, Albin RL, Kuhl DE. Alzheimer's disease versus dementia with Lewy bodies: cerebral metabolic distinction with autopsy confirmation. Ann Neurol 2001;50(3):358-365.

13. Graff-Radford J, Murray ME, Lowe VJ, et al. Dementia with Lewy bodies: basis of cingulate island sign. Neurology 2014;83(9):801-809.

14. Holtbernd F, Gagnon J-F, Postuma RB, et al. Abnormal metabolic network activity in REM sleep behavior disorder. Neurology 2014;82(7):620-627.

15. Eckert T, Tang C, Eidelberg D. Assessment of the progression of Parkinson's disease: a metabolic network approach. Lancet Neurol 2007;6(10):926-932.

16. Huang C, Tang C, Feigin A, et al. Changes in network activity with the progression of Parkinson's disease. Brain 2007;130(Pt 7):1834-1846.

17. Ye BS, Lee S, Yoo H, et al. Distinguishing between dementia with Lewy bodies and Alzheimer's disease using metabolic patterns. Neurobiol Aging 2020;87:11-17.

18. Huber M, Beyer L, Prix C, et al. Metabolic Correlates of Dopaminergic Loss in Dementia with Lewy Bodies. Mov Disord 2020;35(4):595-605.

19. Kang SW, Jeon S, Lee YG, et al. Implication of metabolic and dopamine transporter

PET in dementia with Lewy bodies. Sci Rep 2021;11(1):14394.

20. Petersen RC, Aisen PS, Beckett LA, et al. Alzheimer's Disease Neuroimaging Initiative (ADNI): clinical characterization. Neurology 2010;74(3):201-209.

21. Merdes AR, Hansen LA, Jeste DV, et al. Influence of Alzheimer pathology on clinical diagnostic accuracy in dementia with Lewy bodies. Neurology 2003;60(10):1586-1590.

22. Tiraboschi P, Attems J, Thomas A, et al. Clinicians' ability to diagnose dementia with Lewy bodies is not affected by beta-amyloid load. Neurology 2015;84(5):496-499.

23. Ferman TJ, Aoki N, Boeve BF, et al. Subtypes of dementia with Lewy bodies are associated with alpha-synuclein and tau distribution. Neurology 2020;95(2):e155-e165.

24. Lee YG, Jeon S, Kang SW, et al. Interaction of CSF α-synuclein and amyloid beta in cognition and cortical atrophy. Alzheimers Dement (Amst) 2021;13(1):e12177.

25. Clinton LK, Blurton-Jones M, Myczek K, Trojanowski JQ, LaFerla FM. Synergistic Interactions between Abeta, tau, and alpha-synuclein: acceleration of neuropathology and cognitive decline. J Neurosci 2010;30(21):7281-7289.

26. Hansson O, Seibyl J, Stomrud E, et al. CSF biomarkers of Alzheimer's disease concord with amyloid-beta PET and predict clinical progression: A study of fully automated immunoassays in BioFINDER and ADNI cohorts. Alzheimers Dement 2018;14(11):1470-1481.

27. Cairns NJ, Taylor-Reinwald L, Morris JC, Alzheimer's Disease Neuroimaging I. Autopsy consent, brain collection, and standardized neuropathologic assessment of ADNI participants: the essential role of the neuropathology core. Alzheimers Dement 2010;6(3):274-279.

28. Montine TJ, Phelps CH, Beach TG, et al. National Institute on Aging-Alzheimer's

Association guidelines for the neuropathologic assessment of Alzheimer's disease: a practical approach. Acta Neuropathol 2012;123(1):1-11.

29. McKeith IG, Boeve BF, Dickson DW, et al. Diagnosis and management of dementia with Lewy bodies: Fourth consensus report of the DLB Consortium. Neurology 2017;89(1):88-100.

30. Chatterjee A, Hirsch-Reinshagen V, Moussavi SA, Ducharme B, Mackenzie IR, Hsiung GR. Clinico-pathological comparison of patients with autopsy-confirmed Alzheimer's disease, dementia with Lewy bodies, and mixed pathology. Alzheimers Dement (Amst) 2021;13(1):e12189.

31. Beach TG, Adler CH, Lue L, et al. Unified staging system for Lewy body disorders: correlation with nigrostriatal degeneration, cognitive impairment and motor dysfunction. Acta Neuropathol 2009;117(6):613-634.

32. McKeith IG, Dickson DW, Lowe J, et al. Diagnosis and management of dementia with Lewy bodies: third report of the DLB Consortium. Neurology 2005;65(12):1863-1872.

33. Woolrich MW, Jbabdi S, Patenaude B, et al. Bayesian analysis of neuroimaging data in FSL. Neuroimage 2009;45(1 Suppl):S173-186.

34. Fonov V, Coupe P, Eskildsen S, Collins D. Atrophy-specific MRI brain template for Alzheimer's disease and mild cognitive impairment. Alzheimer's & Dementia: The Journal of the Alzheimer's Association 2011;7(4):S58.

35. Zhang Y, Brady M, Smith S. Segmentation of brain MR images through a hidden Markov random field model and the expectation-maximization algorithm. IEEE transactions on medical imaging 2001;20(1):45-57.

36. Patenaude B, Smith SM, Kennedy DN, Jenkinson M. A Bayesian model of shape and appearance for subcortical brain segmentation. Neuroimage 2011;56(3):907-922.

37. Moeller J, Strother S. A regional covariance approach to the analysis of functional patterns in positron emission tomographic data. Journal of Cerebral Blood Flow & Metabolism 1991;11(1_suppl):A121-A135.

38. Rolls ET, Huang C-C, Lin C-P, Feng J, Joliot M. Automated anatomical labelling atlas 3. NeuroImage 2020;206:116189.

39. Clinton LK, Blurton-Jones M, Myczek K, Trojanowski JQ, LaFerla FM. Synergistic Interactions between Abeta, tau, and alpha-synuclein: acceleration of neuropathology and cognitive decline. The Journal of neuroscience : the official journal of the Society for Neuroscience 2010;30(21):7281-7289.

40. Moussaud S, Jones DR, Moussaud-Lamodière EL, Delenclos M, Ross OA, McLean PJ. Alpha-synuclein and tau: teammates in neurodegeneration? Molecular Neurodegeneration 2014;9(1):43.

41. Teravskis PJ, Covelo A, Miller EC, et al. A53T Mutant Alpha-Synuclein Induces Tau-Dependent Postsynaptic Impairment Independently of Neurodegenerative Changes. J Neurosci 2018;38(45):9754-9767.

42. Peters ST, Fahrenkopf A, Choquette JM, Vermilyea SC, Lee MK, Vossel K. Ablating Tau Reduces Hyperexcitability and Moderates Electroencephalographic Slowing in Transgenic Mice Expressing A53T Human α-Synuclein. Frontiers in Neurology 2020;11:563.

43. Singh B, Covelo A, Martell-Martinez H, et al. Tau is required for progressive synaptic and memory deficits in a transgenic mouse model of alpha-synucleinopathy. Acta Neuropathol 2019;138(4):551-574.

44. Yoo HS, Lee EC, Chung SJ, et al. Effects of Alzheimer's disease and Lewy body disease on subcortical atrophy. Eur J Neurol 2020;27(2):318-326.

45. Kang SW, Jeon S, Yoo HS, et al. Effects of Lewy body disease and Alzheimer disease

on brain atrophy and cognitive dysfunction. Neurology 2019;92(17):e2015-e2026.

46. Lee YG, Jeon S, Yoo HS, et al. Amyloid-beta-related and unrelated cortical thinning in dementia with Lewy bodies. Neurobiol Aging 2018;72:32-39.

47. Shimojo M, Takuwa H, Takado Y, et al. Selective Disruption of Inhibitory Synapses Leading to Neuronal Hyperexcitability at an Early Stage of Tau Pathogenesis in a Mouse Model. J Neurosci 2020;40(17):3491-3501.

48. Ferrer I, Santpere G, van Leeuwen FW. Argyrophilic grain disease. Brain 2008;131(Pt 6):1416-1432.

49. Crary JF, Trojanowski JQ, Schneider JA, et al. Primary age-related tauopathy (PART): a common pathology associated with human aging. Acta Neuropathol 2014;128(6):755-766.

50. Jack CR, Jr. PART and SNAP. Acta Neuropathol 2014;128(6):773-776.

Figure legends

Figure 1. Effects of AD and LBD pathologies on regional brain metabolism. Data are the results of general linear models for regional ^{18}F-FDG metabolism after controlling for age, sex, and education. AD (A), LBD (B), and their interaction term (C) were used as predictors. The color scale indicates effect sizes (r-score) within statistically significant regions after multiple comparisons correction ($p<0.05$, false discovery rate). The brain images are displayed according to neurological convention. AD, Alzheimer's disease; FDG, fluorodeoxyglucose; LBD, Lewy body disease.

Figure 2. Regional brain metabolism of the neuropathologic groups. Data are the results of group comparison for regional ^{18}F-FDG metabolism after controlling for age, sex, and education. Each neuropathologic group was compared to the control group. The color scale indicates effect sizes (Cohen's *d*) within statistically significant regions after multiple comparisons correction ($p<0.05$, false discovery rate). The brain images are displayed according to neurological convention. AD, Alzheimer's disease; FDG, fluorodeoxyglucose; LBD, Lewy body disease.

Figure 3. Regional brain metabolism in the neuropathologic groups. Data shows the distribution of the z-transformed residuals in each neuropathologic group from the general linear models for regional ^{18}F-FDG metabolism after controlling for age, sex, and education. Fifteen regions of interests were selected where significant independent effects or interactions effects between AD and LBD pathologies were identified from Figure 1. ACC, anterior cingulate cortex; AD, Alzheimer's disease; FDG, fluorodeoxyglucose; LBD, Lewy body disease; LBRPs, Lewy body-related metabolic patterns; PCC, posterior cingulate cortex.

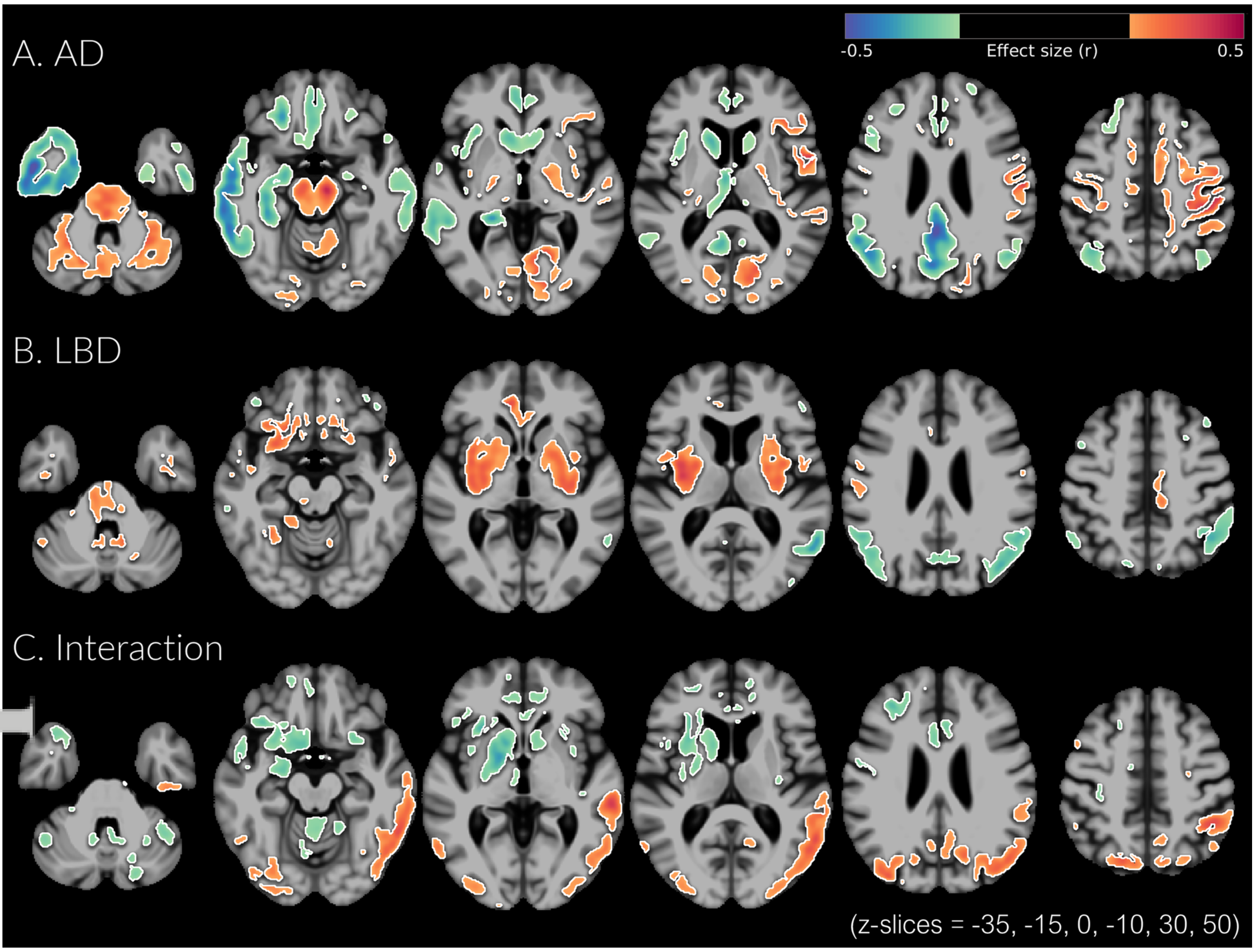

ANA_26355_Figure1.tif

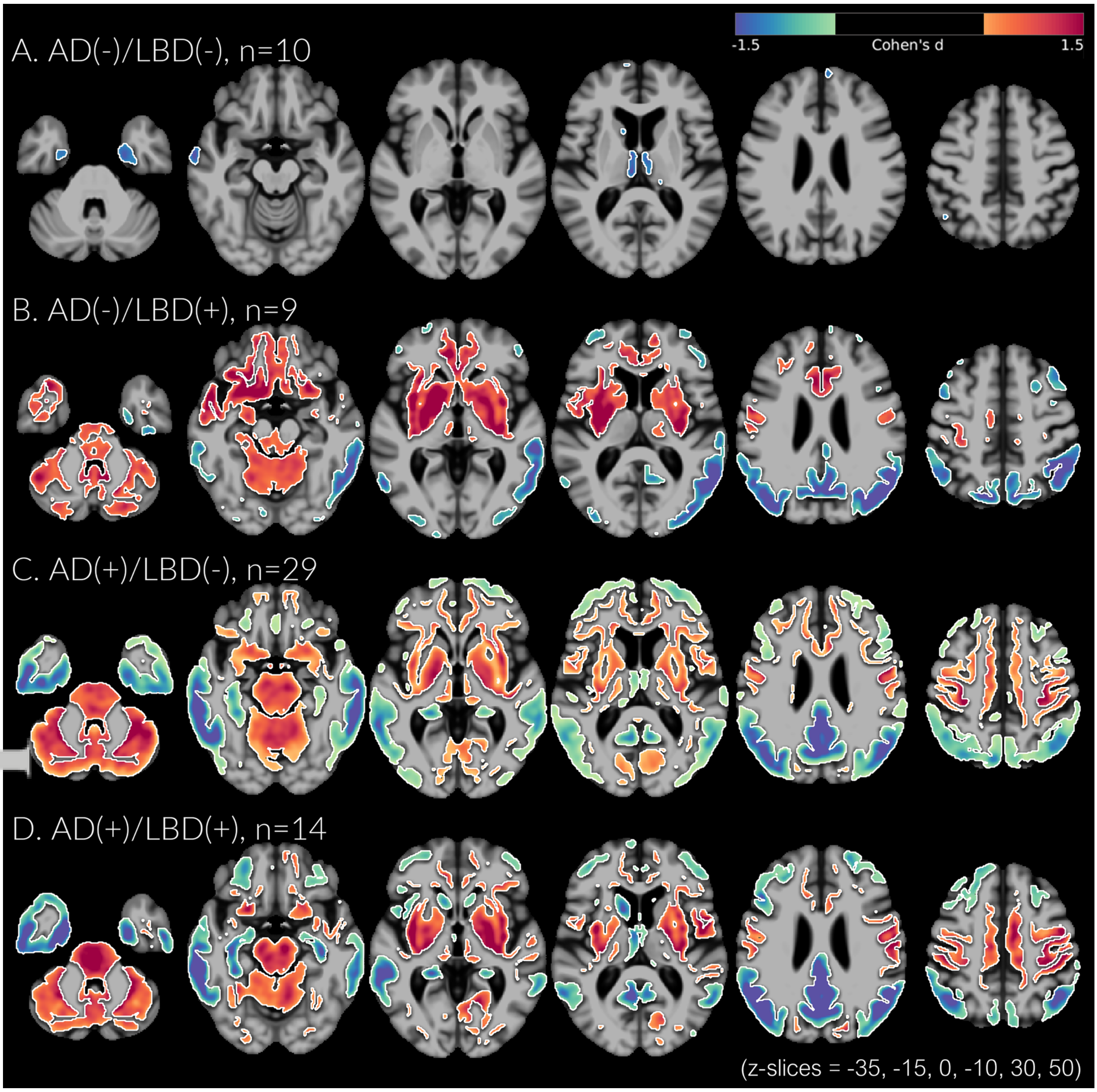

ANA_26355_Figure2.tif

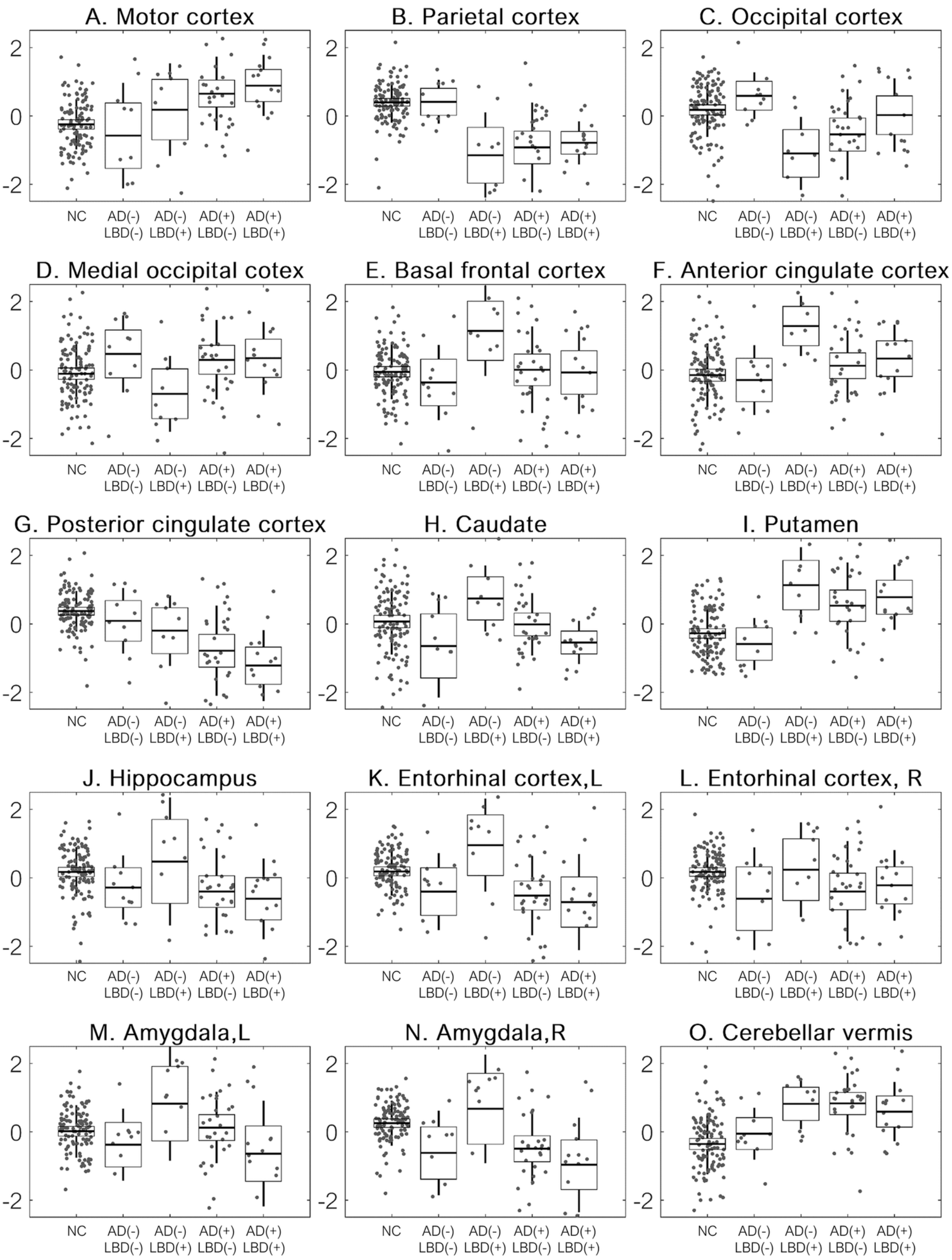

ANA_26355_Figure3.tif

Table 1. Demographic and clinical characteristics of participants

	Control	AD(-)/LBD(-)	AD(-)/LBD(+)	AD(+)/LBD(-)	AD(+)/LBD(+)	*p*
Number	110	10	9	29	14	
Age at PET (y)	76.6 (6.0)	80.0 (6.8)	82.0 (8.8)	78.5 (8.1)	78.0 (6.3)	0.093
Age at autopsy (y)	N/A	85.1 (7.5)	86.9 (8.9)	83.6 (8.6)	82.3 (6.6)	0.563
Interval between PET and autopsy	N/A	5.2 (3.8)	4.9 (3.2)	5.1 (2.7)	4.3 (2.8)	0.874
Sex, female	49 (44.5%)	3 (25.0%)	1 (11.1%)	13 (44.8%)	2 (14.3%)	0.053
Education (y)	16.5 (2.7)	15.9 (2.6)	16.4 (3.5)	16.1 (2.4)	16.6 (2.2)	0.934
MMSE	29.0 (1.4)	27.9 (1.6)	24.4 (3.2)[a, b, c, d]	20.8 (6.0)[a, b, c]	20.4 (5.5)[a, b, d]	<0.001
CDR-SOB	0	1.5 (1.4)	4.1 (3.5)[a, b, d]	6.2 (4.0)[a, b]	6.6 (3.5)[a, b, d]	<0.001

Abbreviations: AD, Alzheimer's disease; CDR-SOB, clinical dementia rating sum of boxes; LBD, Lewy body disease; MMSE, Mini-Mental Status Examination; PET, positron emission tomography.

Data are expressed as the mean (standard deviation) or numbers (%). Results are from the analysis of variance or chi-square tests, as appropriate.

[a]Significantly different in comparison with the control group.

[b]Significantly different in comparison with AD(-)/LBD(-) group.

[c]Significantly different in comparison between AD(-)/LBD(+) and AD(+)/LBD(-) groups.

[d]Significantly different in comparison between AD(-)/LBD(+) and AD(+)/LBD(+) groups.

Table 2. Effects of AD and LBD pathologies on regional metabolic activity shown in Figure 1

Regions	AAL3 label	AD		LBD		Interaction	
		r	p^a	r	p^a	r	p^a
Motor cortex	1, 2	0.28	**< 0.001**	0.14	0.075	-0.05	0.313
Parietal cortex	63 – 70	-0.18	**0.013**	-0.30	**< 0.001**	0.34	**< 0.001**
Occipital cortex	53 – 58	0.07	0.191	-0.14	0.075	0.32	**< 0.001**
Medial occipital cortex	47, 48	0.22	**0.005**	-0.10	0.175	0.11	0.102
Basal frontal cortex	17, 18, 21 – 24	-0.19	**0.013**	0.20	**0.018**	-0.22	**0.005**
Anterior cingulate cortex	151, 152[b]	-0.12	0.080	0.28	**< 0.001**	-0.22	**0.006**
Posterior cingulate cortex	39, 40	-0.38	**< 0.001**	-0.20	**0.015**	0.03	0.368
Cerebellar vermis	113, 114, 120	0.17	**0.024**	0.19	**0.020**	-0.26	**< 0.001**
Caudate	75, 76	-0.21	**0.006**	0.03	0.446	-0.21	**0.008**
Putamen	77 ,78	0.08	0.161	0.31	**< 0.001**	-0.22	**0.005**
Hippocampus	41,42	-0.26	**< 0.001**	0.02	0.451	-0.09	0.151
Entorhinal cortex, L	43[c]	-0.38	**< 0.001**	0.00	0.498	-0.16	**0.028**
Entorhinal cortex, R	44[c]	-0.16	**0.030**	0.05	0.401	0.01	0.453
Amygdala, L	45	-0.22	**0.005**	0.02	0.451	-0.26	**< 0.001**
Amygdala, R	46	-0.11	0.099	0.02	0.451	-0.13	0.069

Abbreviations: AAL3, Automated Anatomical Labelling atlas 3; AD, Alzheimer's disease; and LBD, Lewy body disease.

Data are the results of general linear models for regional ^{18}F-FDG metabolism after controlling for age, sex, and education. AD, LBD, and their interaction term (AD×LBD) were used as predictors.

[a]Corrected *P* values after multiple comparison correction using false discovery rate method.

[b]Subgenual part of ACC on AAL3.

[c]The anterior part of parahippocampal gyrus on AAL3 subdivided in half along the y-axis.

Table 3. Effects of AD and LBD neuropathologies on LBRPs

	AD		LBD		Interaction	
	β (SE)	*p*	β (SE)	*p*	β (SE)	*p*
LBRPs	24.80 (2.69)	<0.001	74.64 (15.74)	<0.001	-25.27 (7.04)	<0.001

Abbreviations: AD, Alzheimer's disease; LBD, Lewy body disease; LBRPs, Lewy body-related metabolic patterns.

Data are the results of general linear models for LBRPs after controlling for age, sex, and education. AD, LBD, and their interaction term (AD×LBD) were used as predictors.